



CHORUS

This is the accepted manuscript made available via CHORUS. The article has been published as:

Linking local structure and properties in perovskites containing equal concentrations of manganese and ruthenium

Graham King, Rebecca A. Ricciardo, Jennifer R. Soliz, Patrick M. Woodward, and Anna Llobet

Phys. Rev. B **83**, 134123 — Published 26 April 2011

DOI: [10.1103/PhysRevB.83.134123](https://doi.org/10.1103/PhysRevB.83.134123)

Linking Local Structure and Properties in Perovskites Containing Equal Concentrations of Manganese and Ruthenium

Graham King¹, Rebecca A. Ricciardo², Jennifer R. Soliz², Patrick M. Woodward², Anna Llobet¹

¹ *Lujan Neutron Scattering Center, Los Alamos National Laboratory, MS H805, Los Alamos, NM 87545, USA*

² *Department of Chemistry, The Ohio State University, 100 West 18th Avenue, Columbus, OH 43210-1185, USA*

Abstract:

The local structures of six perovskite compounds containing equal amounts of manganese and ruthenium on the *B*-site have been investigated by neutron and X-ray pair distribution function analysis. The compounds $\text{SrMn}_{0.5}\text{Ru}_{0.5}\text{O}_3$, $\text{Sr}_{0.5}\text{Ca}_{0.5}\text{Mn}_{0.5}\text{Ru}_{0.5}\text{O}_3$, and $\text{CaMn}_{0.5}\text{Ru}_{0.5}\text{O}_3$ were studied to investigate the effects of pure chemical pressure on the local structure and valency ratio between $\text{Mn}^{3+}/\text{Ru}^{5+}$ and $\text{Mn}^{4+}/\text{Ru}^{4+}$. Reverse Monte Carlo simulations **confirm** that there is a shift in the *B*-site cation charge distribution from nearly equal amounts of Mn^{3+} , Ru^{5+} , Mn^{4+} , and Ru^{4+} for $\text{SrMn}_{0.5}\text{Ru}_{0.5}\text{O}_3$ to primarily Mn^{4+} and Ru^{4+} for $\text{CaMn}_{0.5}\text{Ru}_{0.5}\text{O}_3$. The compounds $\text{Ba}_{0.5}\text{La}_{0.5}\text{Mn}_{0.5}\text{Ru}_{0.5}\text{O}_3$, $\text{Ca}_{0.5}\text{La}_{0.5}\text{Mn}_{0.5}\text{Ru}_{0.5}\text{O}_3$, and $\text{Sr}_{0.5}\text{Ca}_{0.25}\text{La}_{0.25}\text{Mn}_{0.5}\text{Ru}_{0.5}\text{O}_3$ were also investigated to study the effects of changing the charge of the *A*-site cation. Although substitution of La^{3+} for a divalent alkaline earth ion increases the Mn^{3+} content, this series of compounds also shows a relative increase in the concentration of Mn^{4+} as the average size of the *A*-site cation is decreased. **In all compounds** the octahedra containing Mn^{3+} are found to be Jahn-Teller distorted regardless of whether or not long range orbital ordering is observed, **while the Ru-centered octahedra are symmetric**. **No evidence** for short range cation ordering at either the *A* or *B*-sites **was found** for any of the compositions. This study also reports the previously undocumented finding that locally the *A*-site cations lie closer to the Mn ions than to the Ru ions and this asymmetry appears to be correlated to the **degree of octahedral tilting**.

1. Introduction

The interplay between electronic, lattice, and magnetic degrees of freedom is at the origin of the broad variety of emergent phenomena exhibited by mixed metal oxides. Perovskite compounds containing manganese or ruthenium are among the most interesting of these systems. The manganite perovskites have been studied very extensively because they possess many properties of technological importance such as colossal magnetoresistance ($A^{2+}_{1-x}A^{3+}_x\text{MnO}_3$)¹ and multiferroic behavior (BiMnO_3 , TbMnO_3).^{2, 3} There has also been a great deal of research on ruthenate perovskites owing to behaviors such as itinerant electron ferromagnetism (SrRuO_3)^{4, 5} and superconductivity in closely related Ruddlesden–Popper phases (Sr_2RuO_4).⁶

It is therefore not surprising that perovskites which contain both Mn and Ru have also attracted considerable interest.⁷⁻¹⁵ The physical properties of these compounds are primarily governed by the oxidation states of the Mn and Ru cations, which often exist in a state of mixed valency. The properties of these materials can be tuned by controlling the ratio of Mn to Ru and also by manipulating the charge and/or size of the cations on the *A*-site.

This study concerns the local structures of perovskites which have equal amounts of Mn and Ru on the *B*-site ($\text{AMn}_{0.5}\text{Ru}_{0.5}\text{O}_3$). While a considerable amount of work has already been done on such compositions, a clear link between the structure and properties is still missing. Despite the absence of long range order of the Mn and Ru cations, such compounds are found to magnetically order near room temperature.^{7, 16, 17} This is quite different from the spin glass behavior that is typically observed for transition metal compounds that have a disordered arrangement of magnetic ions. The magnetic ordering raises interesting questions about how the magnetic exchange interactions are operating in these compounds. Also, despite the chemical disorder, some of these compositions are found to show long range orbital ordering. The cation disorder and large variety of oxidation states available for both Mn and Ru can be expected to generate a large number of different local bonding environments. It is these local environments that primarily determine the properties of these compounds. Therefore, a study of the local structure is needed to be able to explain their unusual behaviors.

A recent study has found that the valence states of the *B*-site cations can be tuned by changing the size of the *A*-site cation while maintaining a constant *A*-site charge.¹⁷ X-ray

absorption near edge spectroscopy (XANES) measurements on a series of $\text{Sr}_{1-x}\text{Ca}_x\text{Mn}_{0.5}\text{Ru}_{0.5}\text{O}_3$ perovskites have shown that a valence degeneracy between $\text{Mn}^{3+}/\text{Ru}^{5+}$ and $\text{Mn}^{4+}/\text{Ru}^{4+}$ exists across the entire series. The Sr rich samples, which have the largest tolerance factors (τ), crystallize with $I4/mcm$ space group symmetry. This space group permits out-of-phase tilting of the BO_6 octahedra about the c -axis. Such compositions undergo C-type antiferromagnetic ordering and cooperative Jahn-Teller (JT) distortions originating from ordering of the occupied d_{z^2} orbitals. XANES measurements show nearly equal amounts of all four oxidation states: Mn^{3+} (electron configuration: $t_{2g}^3 e_g^1$), Mn^{4+} ($t_{2g}^3 e_g^0$), Ru^{4+} ($t_{2g}^4 e_g^0$) and Ru^{5+} ($t_{2g}^3 e_g^0$). As Ca is substituted for Sr, the tolerance factor is lowered, eventually triggering octahedral tilting about all three axes and lowering the space group symmetry to $Pnma$. The change in symmetry also results in a change from antiferromagnetism to itinerant electron ferromagnetism. The XANES measurements show that as the amount of octahedral tilting increases, there is a shift in the oxidation states of the B -site cations towards $\text{Mn}^{4+}/\text{Ru}^{4+}$. The octahedral tilting causes the B -O- B bond angles to deviate from 180° , which inhibits the cooperative ordering of the long and short bonds of the JT distorted Mn^{3+} . The system responds by shifting electron density away from Mn and onto Ru. It has been proposed that converting some Mn^{3+} to Mn^{4+} helps relieve the local bond strains that result from non-cooperative JT distortions.

The oxidation states of the B -sites cations can also be controlled by changing the average charge of the A -site cation. By replacing half of the divalent A -site cations with La^{3+} , the oxidation states of the B -site cations are lowered, presumably to Mn^{3+} and Ru^{4+} . A number of studies on $A_{0.5}\text{La}_{0.5}\text{Mn}_{0.5}\text{Ru}_{0.5}\text{O}_3$ ($A = \text{Ca}, \text{Sr}, \text{Ba}$) perovskites have been published which show that these compounds order ferromagnetically at temperatures slightly above 200 K.^{16, 18, 19}

There are a number of unanswered questions concerning the local structures of these materials that are crucial to understanding their behavior. Is there any short range ordering of the Mn and Ru cations which is responsible for their unusual orbital ordering and magnetic ordering behavior? What are the local coordination environments of the Mn and Ru cations and how do these correlate with the properties? When long range cooperative JT distortions are lost, do local JT distortions of Mn^{3+} remain? In addition to answering these questions, this study also strives to elucidate the effects of A -site cation size and average A -site charge on the local structures and the mixed valency between Mn and Ru. In order to study the effects of chemical pressure with a

constant *A*-site cation charge, we have studied three members of the $\text{Sr}_{1-x}\text{Ca}_x\text{Mn}_{0.5}\text{Ru}_{0.5}\text{O}_3$ series, $x = 0$ $\text{SrMn}_{0.5}\text{Ru}_{0.5}\text{O}_3$ ($\tau = 0.99$), $x = 0.5$ $\text{Sr}_{0.5}\text{Ca}_{0.5}\text{Mn}_{0.5}\text{Ru}_{0.5}\text{O}_3$ ($\tau = 0.97$), and $x = 1$ $\text{CaMn}_{0.5}\text{Ru}_{0.5}\text{O}_3$ ($\tau = 0.93$). To study the effects of changing the average *A*-site cation charge we have also studied three additional compositions, $\text{Ba}_{0.5}\text{La}_{0.5}\text{Mn}_{0.5}\text{Ru}_{0.5}\text{O}_3$ ($\tau = 0.99$), $\text{Ca}_{0.5}\text{La}_{0.5}\text{Mn}_{0.5}\text{Ru}_{0.5}\text{O}_3$ ($\tau = 0.94$), and $\text{Sr}_{0.5}\text{Ca}_{0.25}\text{La}_{0.25}\text{Mn}_{0.5}\text{Ru}_{0.5}\text{O}_3$ ($\tau = 0.96$). The local structures of these six compounds were investigated using the pair distribution function (PDF) method based on X-ray and neutron total scattering data.

2. Experimental:

Using the conventional ceramic method, polycrystalline samples of $\text{AMn}_{0.5}\text{Ru}_{0.5}\text{O}_3$ ($A = \text{Sr}, \text{Ca}, \text{Sr}_{0.5}\text{Ca}_{0.5}, \text{Ba}_{0.5}\text{La}_{0.5}, \text{Ca}_{0.5}\text{La}_{0.5},$ and $\text{Sr}_{0.5}\text{Ca}_{0.25}\text{La}_{0.25}$) were prepared. Stoichiometric ratio amounts of the starting reagents: BaCO_3 (Mallinckrodt Baker, 99.4% purity), CaCO_3 (Mallinckrodt Baker, 99.95% purity), La_2O_3 (Sigma-Aldrich, 99.99% purity; heated to 900°C for 8h prior to usage and then stored in a desiccator when not in use), Mn_2O_3 (CERAC, 99.9% purity), RuO_2 (Sigma-Aldrich, 99.9% purity), and SrCO_3 (Sigma Aldrich, 99.9+% purity) were accurately weighed, mixed intimately, and ground together using an agate mortar and pestle. The samples were individually loaded into high density (99.8% dense) alumina crucibles and then placed into a high temperature box furnace. Each of the samples was heated to 1385 °C in air for 15h. The products appear as dark gray powders. X-ray powder diffraction, using a Bruker D8 Advance diffractometer with an incident beam monochromator, was used to confirm sample purity.

Neutron total scattering data was collected on the HIPD instrument of the Lujan Neutron Scattering Center of Los Alamos National Laboratory. X-ray total scattering data was collected at the 11-BM beamline of the Advanced Photon Source at Argonne National Laboratory. All data were collected at room temperature. Rietveld refinements were carried out using the GSAS software package.^{20, 21} Reduction of the neutron data to obtain the pair distribution function, $G(r)$, was done using the program PDFgetN with a Q_{max} of 30 \AA^{-1} .²² The intensities of the X-ray powder diffraction rings were integrated with the program FIT2D.^{23, 24} Reduction of the X-ray data was done using the program PDFgetX2 with a Q_{max} of 24 \AA^{-1} .²⁵ In this study we use the

following definition of the pair distribution function: $G(r) = 4\pi r[\rho(r) - \rho_0]$, where $\rho(r)$ is the microscopic pair density, ρ_0 is the average pair density, and r is the radial distribution. Modeling of the $G(r)$ functions was done using the programs PDFgui and RMCProfile.^{26,27}

3. Results and Discussion:

3.1. Average Crystal Structures

The first step towards understanding the local structures of these materials is determining the average long range structures. In order to solve the crystal structures Rietveld refinements were performed on the neutron powder diffraction (NPD) patterns of all compounds. There was no evidence of any long range Mn/Ru cation ordering for any of the compositions.

The crystal structure of $\text{SrMn}_{0.5}\text{Ru}_{0.5}\text{O}_3$ has been reported by several groups of researchers to have tetragonal $I4/mcm$ space group symmetry.^{11, 16, 17, 28, 29} This space group allows for out-of-phase rotations of the octahedra about the c -axis, corresponding to the $a^0a^0c^-$ Glazer tilt system. A slight elongation of the B -O bonds pointing along the c -axis relative to those in the a - b plane has been reported and attributed to cooperative JT distortions of the octahedra containing Mn^{3+} ions. Our results match closely with the previously reported structures, confirming $I4/mcm$ space group symmetry. In this space group the B -O- B bond angle along the c -axis is restricted by symmetry to be 180° . The B -O- B bond angles within the a - b plane refined to be $167.26(1)^\circ$. The B -O bonds along the c -axis were refined to be 0.036 \AA longer than those in the ab -plane.

Our Rietveld refinement results show that $\text{Ba}_{0.5}\text{La}_{0.5}\text{Mn}_{0.5}\text{Ru}_{0.5}\text{O}_3$ also has $I4/mcm$ space group symmetry. Earlier reports based on laboratory X-ray diffraction data reported this compound as having cubic $Pm\bar{3}m$ symmetry.³⁰ A later NPD study reported the structure as having orthorhombic $Pnma$ symmetry.¹⁸ However, in this study the B -O- B bond angle along the c -axis is reported as $175.4(4)^\circ$, which is quite close to 180° . This could be taken as an indication that a higher symmetry solution was missed. A synchrotron X-ray powder diffraction study has also been conducted which also concluded that $Pnma$ was the correct space group.³¹ However, in this study only $Pm\bar{3}m$ and $Pnma$ models were tested and intermediate symmetries were not

considered. The NPD pattern from our study shows supercell reflections that cannot be indexed with a cubic space group, thereby ruling out $Pm\bar{3}m$ as a possibility. All peaks could be indexed using space group $I4/mcm$. Rietveld refinements in this space group are able to provide a good fit to all peak intensities. Refinements were also done in space group $Pnma$, but these failed to provide any improvement over the higher symmetry $I4/mcm$ refinements. The assignment of $I4/mcm$ symmetry seems more likely considering that the tolerance factor of this composition is very close to 1. $Pnma$ symmetry, with octahedral tilting in all three directions, is only expected for smaller tolerance factors.

The results of the $Ba_{0.5}La_{0.5}Mn_{0.5}Ru_{0.5}O_3$ refinement show the $B-O-B$ bond angle within the $a-b$ plane to be $169.42(3)^\circ$, similar to that found in $SrMn_{0.5}Ru_{0.5}O_3$. Unlike $SrMn_{0.5}Ru_{0.5}O_3$, there is no elongation of the bonds along the c -axis. The two $B-O$ bond lengths of $1.9917(2)$ Å and $1.9955(6)$ Å are essentially equal (a difference of only 0.004 Å). This is somewhat surprising considering that these compounds both have the same space group symmetry. Furthermore, the $Ba_{0.5}La_{0.5}Mn_{0.5}Ru_{0.5}O_3$ structure **might be** expected to show a greater elongation of the c -axis originating from cooperative JT distortions, **given the fact that** its concentration of Mn^{3+} is about twice that of $SrMn_{0.5}Ru_{0.5}O_3$ ($\sim 50\%$ vs. $\sim 25\%$ **Mn^{3+} on the B -site**). Apparently, higher concentrations of Mn^{3+} do not necessarily lead to an increase in orbital ordering.

The other four compounds studied all have $Pnma$ space group symmetry. This space group corresponds to $a^-b^+a^-$ octahedral tilting. The additional octahedral rotations are the result of the smaller tolerance factors of these compositions. The crystal structures of $Sr_{0.5}Ca_{0.5}Mn_{0.5}Ru_{0.5}O_3$, $CaMn_{0.5}Ru_{0.5}O_3$, and $Ca_{0.5}La_{0.5}Mn_{0.5}Ru_{0.5}O_3$ have been reported before and our results are in close agreement with the previously published results.^{17, 18} The structure of $Sr_{0.5}Ca_{0.25}La_{0.25}Mn_{0.5}Ru_{0.5}O_3$ is reported for the first time. The $B-O$ bond lengths in $Sr_{0.5}Ca_{0.5}Mn_{0.5}Ru_{0.5}O_3$ suggest a cooperative JT distortion, but unlike $SrMn_{0.5}Ru_{0.5}O_3$, it is the $d_{x^2-y^2}$ orbitals that seem to be populated. For the other three compounds there is little indication of any orbital ordering. The differences between the three different $B-O$ bond lengths are less than 0.02 Å in all three cases. Crystallographic information is given in Table 1. The structures of all compounds are available as CIF files in the supporting information.³²

3.2 Comparison of the Local and Average Structures

In order to establish how the local structures differ from the long range averages, the average structures as obtained from the Rietveld refinements were used as starting models for refinements of the PDFs of each compound. Refinements were done using the program PDFgui over r ranges of 1-10 Å, 10-20 Å, and 20-40 Å to test the models at different length scales. In general, the average structures were able to fit the experimental $G(r)$ functions fairly well. The fit of the neutron PDF of $\text{SrMn}_{0.5}\text{Ru}_{0.5}\text{O}_3$ is shown in Figure 1 as a representative example. There are two regions of the $G(r)$'s that are not fit well by the average structures for any of the compounds. As might be expected, the shapes of the first peaks in the $G(r)$'s, centered at ~ 1.95 Å, were not being modeled correctly (Figure 2). This peak corresponds to the Mn–O and Ru–O nearest neighbor distances. The other region where the fit is poor is centered at about 3.35 Å and corresponds to the nearest neighbor A -site cation to B -site cation distance (Figure 3). All the features of the $G(r)$ functions above ~ 3.8 Å were properly modeled by the average structures demonstrating that the deviations from the average structure are very short range and do not tend to correlate beyond one unit cell.

3.2 Local Cation Ordering

Earlier experiments using X-ray, neutron, and electron diffraction have failed to find any signs of Mn/Ru long range cation ordering on the B -sites.¹⁷ Various models have been proposed to explain the magnetic behavior of these compounds, some of which assume short range cation ordering and others which assume a completely random distribution.^{16, 17} Short range ordering of these cations would directly affect the orbital interactions and the magnetic exchange, having important implications for the magnetic and transport properties. Experimentally determining if such short range order exists is therefore essential to being able to rationalize these properties.

In order to test for the presence of short range Mn/Ru cation ordering the average structural models were modified to include cation ordering and were fitted against the low r (1-10 Å) regions of the neutron and X-ray PDFs. Three types of cation ordering were considered: rock-salt, layered, and columnar. The fits to the X-ray $G(r)$'s proved to be nearly insensitive to cation ordering. The change in the R_w of the X-ray fits upon introducing cation ordering was

never more than 4%. Since the neutron scattering lengths of Mn and Ru have opposite signs and a greater difference in scattering power compared to X-rays, the neutron PDFs are a highly sensitive probe of Mn/Ru cation ordering. Introducing cation ordering of any type always resulted in a significant worsening of the fit to the neutron $G(r)$. For the various compositions the rock-salt ordered models increased the R_w anywhere from 29.2-102.6% compared to the models with a random distribution. Similarly, the layered models increased the R_w by 22.8-35.0% and the columnar models increased the R_w by 24.2-34.9 %. These results **strongly suggest** that there is no local B -site cation ordering and that the Mn and Ru distribution is random even at the nearest neighbor length scale.

For compositions with two distinct A -site cations a similar procedure was undertaken. For $\text{Sr}_{0.5}\text{Ca}_{0.5}\text{Mn}_{0.5}\text{Ru}_{0.5}\text{O}_3$ it is difficult to evaluate if there is A -site cation ordering since the scattering powers of Sr and Ca are not drastically different for either neutrons or X-rays. However, the cation ordered models did always provide a worse fit compared to a random distribution. The neutron fits worsened by about 1% while the X-ray fits worsened by up to 2%. For the $\text{Ba}_{0.5}\text{La}_{0.5}\text{Mn}_{0.5}\text{Ru}_{0.5}\text{O}_3$ compound the X-ray PDF is not useful as Ba and La are isoelectronic. The neutron scattering lengths are also similar but do provide a small amount of contrast. The cation ordered models tended to increase the R_w by about 1%. For $\text{Ca}_{0.5}\text{La}_{0.5}\text{Mn}_{0.5}\text{Ru}_{0.5}\text{O}_3$ there is significant contrast for both the X-ray and neutron scattering lengths of Ca and La. Cation ordering increases the R_w of the fit to the neutron PDF by about 2% and the X-ray PDF by 7.5% to 30%, depending on the type of order. These results would seem to indicate that no short range A -site cation ordering is present in any of these three compounds. Local A -site cation ordering in $\text{Sr}_{0.5}\text{Ca}_{0.25}\text{La}_{0.25}\text{Mn}_{0.5}\text{Ru}_{0.5}\text{O}_3$ was not tested since simple ordering schemes are not compatible with the cation ratio, but it is very likely that there is no local ordering present in this compound either.

3.3 RMC Simulations

In order to understand and model the poorly fit features of the $G(r)$ functions a number of structural models were refined using PDFgui. However, we were unable to model the PDFs using any “small box” model which consisted of only a few unit cells. This is most likely due to

there being a large number of different local environments which cannot be represented by such simple models. We therefore attempted modeling the experimental $G(r)$'s using "large box" Reverse Monte Carlo (RMC) simulations to gain further information about the local bonding environments. The starting points for the atomic positions in these refinements were the atomic positions of the average structures. The crystallographic unit cells were expanded into $8 \times 8 \times 8$ supercells each containing 10,240 atoms. The program was initially run using just the atom swap feature in order to generate random distributions of the A and B -site cations before allowing the atoms to move. The Mn–O and Ru–O nearest neighbor atoms were restricted to have inter-atomic distances ranging between 1.7 and 2.35 Å. The maximum move per step was set at 0.01 Å for Mn and Ru and 0.02 Å for all other atoms. The model was fit against the neutron $S(Q)$ and $G(r)$ functions. The simulations were each run for 18 hours on a computer with a 2.3 GHz processor. The resulting fit for the $\text{SrMn}_{0.5}\text{Ru}_{0.5}\text{O}_3$ data is shown in Figure 4.

3.4 Mn and Ru Coordination Environments

Before discussing the results of the RMC refinements it is first helpful to review what sort of Mn and Ru oxidation states and bond distances might be expected. Previous XANES measurements reported that in the $\text{Sr}_{1-x}\text{Ca}_x\text{Mn}_{0.5}\text{Ru}_{0.5}\text{O}_3$ compositions four different oxidation states exist for the B -site cations: Mn^{3+} , Mn^{4+} , Ru^{4+} , and Ru^{5+} .¹⁷ For the pure Sr compound all four oxidation states exist in roughly equal proportions. As more Ca was introduced there was a shift toward $\text{Mn}^{4+}/\text{Ru}^{4+}$. In the $\text{Ba}_{0.5}\text{La}_{0.5}\text{Mn}_{0.5}\text{Ru}_{0.5}\text{O}_3$ and $\text{Ca}_{0.5}\text{La}_{0.5}\text{Mn}_{0.5}\text{Ru}_{0.5}\text{O}_3$ samples it is expected that the oxidation states are Mn^{3+} and Ru^{4+} . For the related compound $\text{Sr}_{0.5}\text{La}_{0.5}\text{Mn}_{0.5}\text{Ru}_{0.5}\text{O}_3$ these oxidation states have been confirmed by XANES measurements.¹⁹ The $\text{Sr}_{0.5}\text{Ca}_{0.25}\text{La}_{0.25}\text{Mn}_{0.5}\text{Ru}_{0.5}\text{O}_3$ oxidation states are less certain, but should range between $\text{Mn}^{3+}/\text{Ru}^{4.5+}$ and $\text{Mn}^{3.5+}/\text{Ru}^{4+}$.

In oxides Ru^{4+} and Ru^{5+} tend to form regular octahedra with very similar average Ru–O bond distances of 1.984 and 1.968 Å, respectively. In contrast, the Mn^{3+} and Mn^{4+} oxidation states have quite different average bond distances. Mn^{4+} is expected to have a symmetric coordination environment with an average Mn–O bond length of 1.903 Å. The average Mn^{3+} bond length is 2.016 Å, but the Mn^{3+} octahedra are expected to exhibit a Jahn-Teller **distortion**,

which usually leads to an elongation of two opposite bonds of the octahedron coupled with some degree of shortening of the remaining four bonds. The long Mn–O bonds typically range in length from 2.15-2.23 Å while the short Mn–O bonds typically range from 1.90-1.97 Å.

One way to analyze the local bonding environments of the Mn and Ru is to examine the Mn–O and Ru–O partial pair distribution functions (PPDF). A PPDF gives the distribution of inter-atomic distances for only a single pair of atoms. The PPDF that are given as output by RMCProfile are not weighted by the scattering power of the elements like an experimental PPDF would be and therefore simply represent the distribution of distances for a particular pair of atoms. The PPDFs of each composition are shown in Figure 5. Simple observation reveals trends common to all compositions. The distribution of Ru–O distances is always much narrower than the distribution of Mn–O distances. The Ru–O distance distributions can be approximated as Gaussian and there are only small differences in the shapes of the Ru–O PPDFs between different compositions. The slight upturn in the number of Ru–O distances at very short and very long lengths is probably due to bunching effects caused by the distance constraints as well as the effects of the termination ripples and is unlikely physical. In contrast, the Mn–O distance distributions are much broader and not Gaussian in shape. There is also significant variation in the distribution of Mn–O inter-atomic distances between the various compositions.

To gain a better understanding of the implications of the PPDFs bond valence sums (BVS) were calculated for every Mn and Ru atom within each supercell. **In calculating bond valence sums the mixed valency presents a slight complication due to the fact that bond valence parameters change slightly with oxidation state.** The bond valence parameters R_{ij} are well established for three of the ions in question: Mn^{3+} ($R_{ij} = 1.760 \text{ \AA}$), Mn^{4+} ($R_{ij} = 1.753 \text{ \AA}$) and Ru^{4+} ($R_{ij} = 1.834 \text{ \AA}$),³³ whereas the same cannot be said for Ru^{5+} . Given the similarity in the bond valence parameters of Mn^{3+} and Mn^{4+} and the uncertainty in the bond valence parameter for Ru^{5+} we elected to use the R_{ij} values Mn^{4+} and Ru^{4+} for all calculations. The average BVS for Mn and Ru ions in each composition are listed in Table 2.

The Mn–O PPDFs of the three $\text{Sr}_{1-x}\text{Ca}_x\text{Mn}_{0.5}\text{Ru}_{0.5}\text{O}_3$ compounds show a decrease in the number of long Mn–O bonds and an increase in the number of short Mn–O bonds as x increases. Since the number of long bonds can be assumed to be related to the concentration of Mn^{3+} and the number of short bonds related to the concentration of Mn^{4+} , this trend represents a shift

towards more Mn^{4+} as the tolerance factor is lowered. The BVS calculations show that the BVS of Mn increases significantly upon going from $\text{SrMn}_{0.5}\text{Ru}_{0.5}\text{O}_3$ to $\text{CaMn}_{0.5}\text{Ru}_{0.5}\text{O}_3$ and the BVS of Ru decreases, confirming the previously reported XANES measurements.

Although the $\text{Ba}_{0.5}\text{La}_{0.5}\text{Mn}_{0.5}\text{Ru}_{0.5}\text{O}_3$ composition is expected to have Mn primarily in the +3 oxidation state, the average structure did not show any signs of a cooperative JT distortion. The BVS analysis confirms that the predominant oxidation state for Mn is 3+ and that Ru is predominately in the +4 oxidation state. If the Mn^{3+} were not JT distorted locally, then the expected shape of the Mn–O PPDF would be a single Gaussian. However, the Mn–O PPDF of $\text{Ba}_{0.5}\text{La}_{0.5}\text{Mn}_{0.5}\text{Ru}_{0.5}\text{O}_3$ is shaped like a double Gaussian, showing a large number of short and long Mn–O bonds, and fewer around the average Mn–O distance. This shows that locally the Mn^{3+} ions are heavily JT distorted.

Since the average *B*-site oxidation state for $\text{Ca}_{0.5}\text{La}_{0.5}\text{Mn}_{0.5}\text{Ru}_{0.5}\text{O}_3$ and $\text{Ba}_{0.5}\text{La}_{0.5}\text{Mn}_{0.5}\text{Ru}_{0.5}\text{O}_3$ should be the same, it might be expected that they would have similar PPDFs and BVS. However, the BVS results show that $\text{Ca}_{0.5}\text{La}_{0.5}\text{Mn}_{0.5}\text{Ru}_{0.5}\text{O}_3$ has a considerably larger Mn BVS than $\text{Ba}_{0.5}\text{La}_{0.5}\text{Mn}_{0.5}\text{Ru}_{0.5}\text{O}_3$. The Mn average BVS of 3.33 for $\text{Ca}_{0.5}\text{La}_{0.5}\text{Mn}_{0.5}\text{Ru}_{0.5}\text{O}_3$ indicates that some Mn^{4+} is also present. It is also apparent by examining the PPDFs that $\text{Ca}_{0.5}\text{La}_{0.5}\text{Mn}_{0.5}\text{Ru}_{0.5}\text{O}_3$ has fewer long Mn–O bonds than does $\text{Ba}_{0.5}\text{La}_{0.5}\text{Mn}_{0.5}\text{Ru}_{0.5}\text{O}_3$, an observation that is also consistent with the presence of some Mn^{4+} . The reduction in the concentration of Mn^{3+} as the tolerance factor decreases on going from $\text{Ba}_{0.5}\text{La}_{0.5}\text{Mn}_{0.5}\text{Ru}_{0.5}\text{O}_3$ to $\text{Ca}_{0.5}\text{La}_{0.5}\text{Mn}_{0.5}\text{Ru}_{0.5}\text{O}_3$ parallels the trend seen for the $\text{Sr}_{1-x}\text{Ca}_x\text{Mn}_{0.5}\text{Ru}_{0.5}\text{O}_3$ series. As there are still a fairly large number of very long Mn–O bonds for $\text{Ca}_{0.5}\text{La}_{0.5}\text{Mn}_{0.5}\text{Ru}_{0.5}\text{O}_3$ it appears as if the Mn^{3+} centered octahedra in this compound are also locally JT distorted despite the lack of long range orbital order. As there are no indications of cation vacancies the most likely mechanism of maintaining charge balance would be the formation of some Ru^{3+} . Indeed, the average Ru BVS does suggest that some Ru^{3+} is present.

Simple charge balance considerations reveal that the average oxidation state of Mn in $\text{Sr}_{0.5}\text{Ca}_{0.25}\text{La}_{0.25}\text{Mn}_{0.5}\text{Ru}_{0.5}\text{O}_3$ should lie between 3+ and 3.5+. The PPDF and BVS analysis of $\text{Sr}_{0.5}\text{Ca}_{0.25}\text{La}_{0.25}\text{Mn}_{0.5}\text{Ru}_{0.5}\text{O}_3$ show that the Mn oxidation state does lie within this range, and is considerably closer to the 3.5+ limit, the average BVS being 3.38. This result is consistent with the trend observed for the other compositions in which the system attempts to minimize its

concentration of Mn^{3+} when the octahedral tilting is large. In this compound there are also a fair number of very long Mn–O bonds which means the Mn^{3+} that is present is most likely locally JT distorted.

The narrow distribution of Ru–O distances for all compositions shows that the JT distortions of the Mn^{3+} ions do not cause any significant distortion of the Ru coordination environment. Since the Ru–O distance distributions appear close to Gaussian in shape, they were fit by Gaussian functions in order to extract an average Ru–O bond length. The results are shown in Table 2. While the average Ru–O bond lengths do not differ greatly among the various compositions, the subtle differences do show a trend. As would be expected, the shorter average Ru–O bond lengths correspond to larger Ru BVS sums.

3.5 Mn–*A* and Ru–*A* Correlation

The RMC simulations show that there is a clear tendency for the *A*-site cations to lie closer to the Mn ions than to the Ru ions. By examining the PPDF in the *r*-range of the nearest neighbor *A*–*B* distances it becomes obvious that the Mn–*A* and Ru–*A* distance distributions are centered at different average distances (Figure 6). This effect is not observed to any appreciable degree at second nearest neighbor distances and beyond. This feature could not be captured by the average structure since it is not consistent with the long range crystal symmetry, indicating that the shift is non-coherent throughout the structure. While a distinct difference between the Mn–*A* and Ru–*A* nearest neighbor distances exists for all compositions, the magnitude of the difference varies considerably.

In order to quantify the typical Mn–*A* and Ru–*A* distances the PPDFs in the *r* range of the nearest neighbor distances were fitted by Gaussian curves. The results are shown in Table 3. Simple electrostatic considerations would suggest that it should be favorable for the *A*-site cations to lie closer to the Mn than to the Ru since for all compositions the Ru is on average more highly charged than the Mn. As the distribution of Mn and Ru is random, these shifts do not have any correlation with each other and are not observed in the average structure. The magnitude of the difference between the Mn–*A* and Ru–*A* distances does not correlate with the magnitude of the differences in charge between the *A* or *B*-site cations among the different

compounds, indicating that electrostatics is not the only force at work. Differences in cation size among the various compounds also do not correlate with the Mn–*A* and Ru–*A* distance difference. The one structural feature that does correlate fairly well with the Mn–*A* and Ru–*A* distance difference is the magnitude of the octahedral tilting. A plot of the $d_{\text{Ru}-A}(\text{ave}) - d_{\text{Mn}-A}(\text{ave})$ vs. the average *B*–*O*–*B* bond angle is shown in Figure 7. Exactly why less octahedral tilting seems to favor a larger difference between the Mn–*A* and Ru–*A* distances is still not completely clear. It could be that as the octahedral tilting increases the *A*-site cation loses the freedom to choose the direction of its shift, as the collapse of the cuboctahedral coordination environment increasingly dictates the direction of its displacement.

4. Conclusions

We have examined the local structures of six perovskites which contain equal amounts of manganese and ruthenium on the *B*-site using the pair distribution function method. Our local structure study shows that the Mn and Ru cations are completely disordered even at very short length scales. The oxidation states and coordination environments of the Mn and Ru cations have also been examined. A previous observation by XANES measurements suggesting a transfer of electron density from manganese to ruthenium as the tolerance factor decreases, thereby shifting the valence degeneracy toward Mn⁴⁺/Ru⁴⁺, is confirmed by the PDF analysis. We find that the octahedra containing Mn³⁺ ions always appear to be locally Jahn-Teller distorted whether or not long range orbital ordering is observed. The Ru coordination environment appears to remain highly symmetric and is not distorted by the presence of the asymmetric Mn³⁺ octahedra. We also find the *A*-site cations tend to lie closer to the Mn ions than to the Ru ions, a trend that becomes less pronounced as the magnitude of the octahedral tilting increases.

Acknowledgements

This work has benefited from the use of HIPD at the Lujan Center at Los Alamos Neutron Science Center, funded by DOE Office of Basic Energy Sciences. Los Alamos National Laboratory is operated by Los Alamos National Security LLC under DOE Contract DE-AC52 06NA25396. Use of the Advanced Photon Source at Argonne National Laboratory was supported by the U. S. Department of Energy, Office of Science, Office of Basic Energy Sciences, under Contract No. DE-AC02-06CH11357. Patrick Woodward, Rebecca Ricciardo, and Jennifer Soliz acknowledge the Center for Emergent Materials at the Ohio State University, an NSF MRSEC (Award Number DMR-0820414), for providing funding for this research. . We would also like to thank Daniel Shoemaker for assistance with the RMC simulations.

	Sr	Sr _{0.5} Ca _{0.5}	Ca	Ba _{0.5} La _{0.5}	Ca _{0.5} La _{0.5}	Sr _{0.5} Ca _{0.25} La _{0.25}
Space Group	<i>I4/mcm</i>	<i>Pnma</i>	<i>Pnma</i>	<i>I4/mcm</i>	<i>Pnma</i>	<i>Pnma</i>
a (Å)	5.4558(1)	5.4660(3)	5.4302(1)	5.6201(1)	5.5335(1)	5.5061(2)
b (Å)		7.7171(4)	7.5989(2)		7.7634(2)	7.7839(3)
c (Å)	7.9083(2)	5.4581(3)	5.3492(1)	7.9670(3)	5.4852(1)	5.5207(2)
V (Å ³)	235.39(1)	230.23(1)	220.73(1)	251.64(1)	235.64(1)	236.61(1)
B-O ₁ (Å)	2 × 1.9771(1)	2 × 1.9335(9)	2 × 1.9464(2)	2 × 1.9917(1)	2 × 1.9855(2)	2 × 1.9648(9)
B-O ₂₍₁₎ (Å)	4 × 1.9409(3)	2 × 1.9633(2)	2 × 1.9614(4)	4 × 1.9955(6)	2 × 1.9912(5)	2 × 1.9781(2)
B-O ₂₍₂₎ (Å)		2 × 1.9760(9)	2 × 1.9625(4)		2 × 2.0025(5)	2 × 1.9783(9)
B-O ₁ - <B-O ₂ >	0.0362	-0.0362	-0.0156	-0.0038	-0.0114	-0.0134
B-O-B _{ax} (°)	180	158.64(1)	154.85(1)	180	155.64(1)	159.31(1)
B-O-B _{eq} (°)	167.26(1)	162.16(5)	152.46(2)	169.42(3)	154.57(3)	162.78(5)

Table 1. Crystallographic data for the $AMn_{0.5}Ru_{0.5}O_3$ perovskites listed by their *A*-site composition. In all cases $Z = 2$.

	Average Mn/Ru Ox. State	Tolerance factor	Average Mn BVS	Average Ru BVS	Average Ru-O distance (Å)
SrMn _{0.5} Ru _{0.5} O ₃	+4	0.99	3.50	4.42	1.950(2)
Sr _{0.5} Ca _{0.5} Mn _{0.5} Ru _{0.5} O ₃	+4	0.97	3.48	4.36	1.967(1)
CaMn _{0.5} Ru _{0.5} O ₃	+4	0.93	3.67	4.26	1.973(1)
Sr _{0.5} Ca _{0.25} La _{0.25} Mn _{0.5} Ru _{0.5} O ₃	+3.75	0.96	3.38	4.08	1.978(2)
Ba _{0.5} La _{0.5} Mn _{0.5} Ru _{0.5} O ₃	+3.5	0.99	3.11	4.01	1.996(2)
Ca _{0.5} La _{0.5} Mn _{0.5} Ru _{0.5} O ₃	+3.5	0.94	3.33	3.92	1.999(2)

Table 2. The average oxidation states of the *B*-site cations (Ox. State), the tolerance factors, the bond valence sums (BVS) for the Mn and Ru cations, and the average Ru-O bond distances.

	Tolerance factor	Mn- <i>A</i> distance (Å)	Ru- <i>A</i> distance (Å)	Difference (Å)
Ba _{0.5} La _{0.5} Mn _{0.5} Ru _{0.5} O ₃	0.99	3.397(4)	3.465(3)	0.067(4)
SrMn _{0.5} Ru _{0.5} O ₃	0.99	3.328(3)	3.389(3)	0.061(3)
Sr _{0.5} Ca _{0.5} Mn _{0.5} Ru _{0.5} O ₃	0.97	3.307(3)	3.357(3)	0.050(3)
Sr _{0.5} Ca _{0.25} La _{0.25} Mn _{0.5} Ru _{0.5} O ₃	0.96	3.333(4)	3.387(4)	0.054(4)
Ca _{0.5} La _{0.5} Mn _{0.5} Ru _{0.5} O ₃	0.94	3.339(4)	3.364(4)	0.025(4)
CaMn _{0.5} Ru _{0.5} O ₃	0.93	3.258(3)	3.285(3)	0.028(3)

Table 3. The Mn to *A*-site cation and Ru to *A*-site cation nearest neighbor distances and the differences between them. The values were obtained by fitting the PDF partials with a Gaussian curve and taking the peak of the curve.

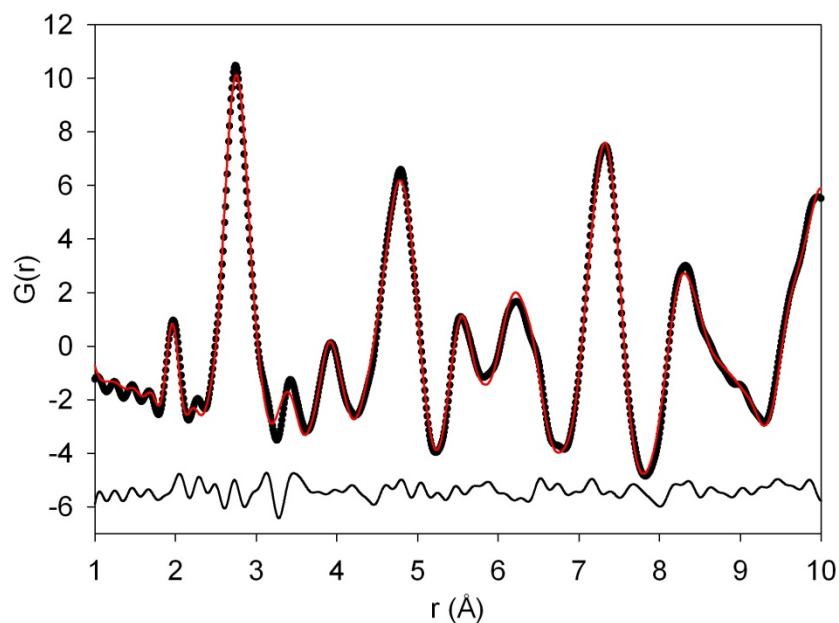


Figure 1. The fit to the neutron $G(r)$ of SrMn_{0.5}Ru_{0.5}O₃ in the range of 1-10 Å using the average long range structure as a model. The black circles are the data points, the red line is the fit, and the difference is shown beneath.

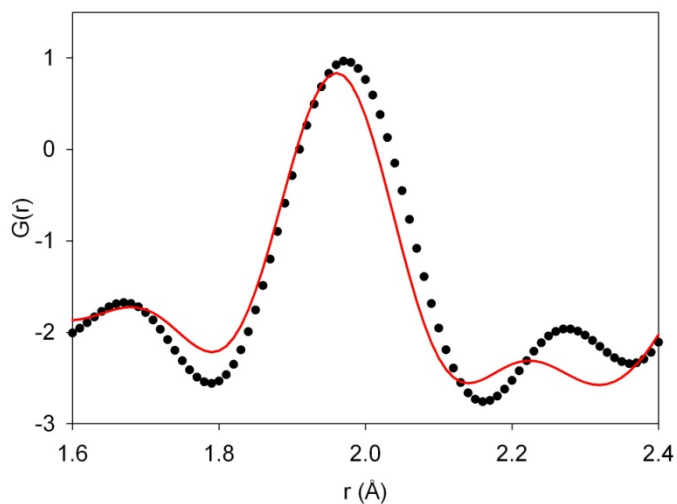


Figure 2. The fit to the $G(r)$ of $\text{SrMn}_{0.5}\text{Ru}_{0.5}\text{O}_3$ in the r range of the nearest neighbor Mn-O and Ru-O distances using the average long range structure as a model. The black circles are the data points and the red line is the fit.

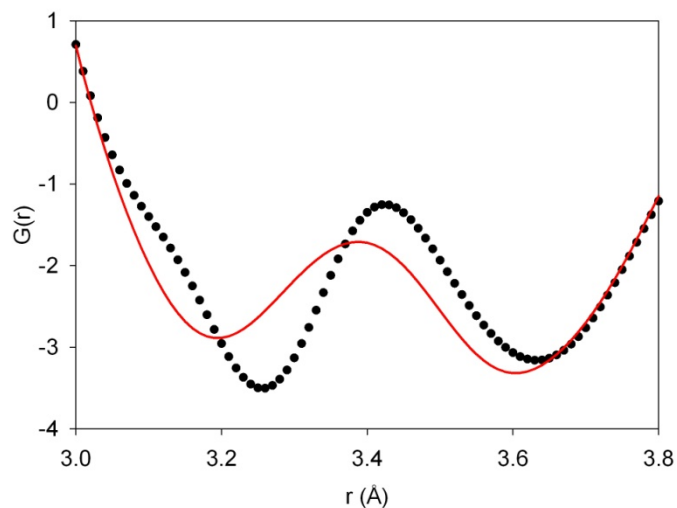


Figure 3. The fit to the $G(r)$ of $\text{SrMn}_{0.5}\text{Ru}_{0.5}\text{O}_3$ in the r range of the nearest neighbor Sr-Mn and Sr-Ru distances using the average long range structure as a model. The black circles are the data points and the red line is the fit.

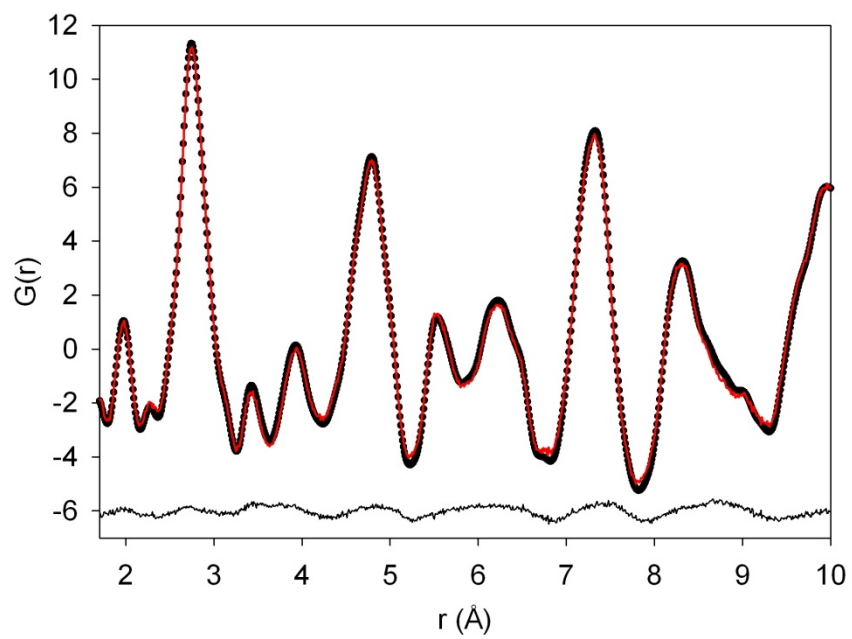


Figure 4. The fit to the $G(r)$ of $\text{SrMn}_{0.5}\text{Ru}_{0.5}\text{O}_3$ resulting from the RMC modeling. The black circles are the data points, the red line is the fit, and the difference is shown beneath.

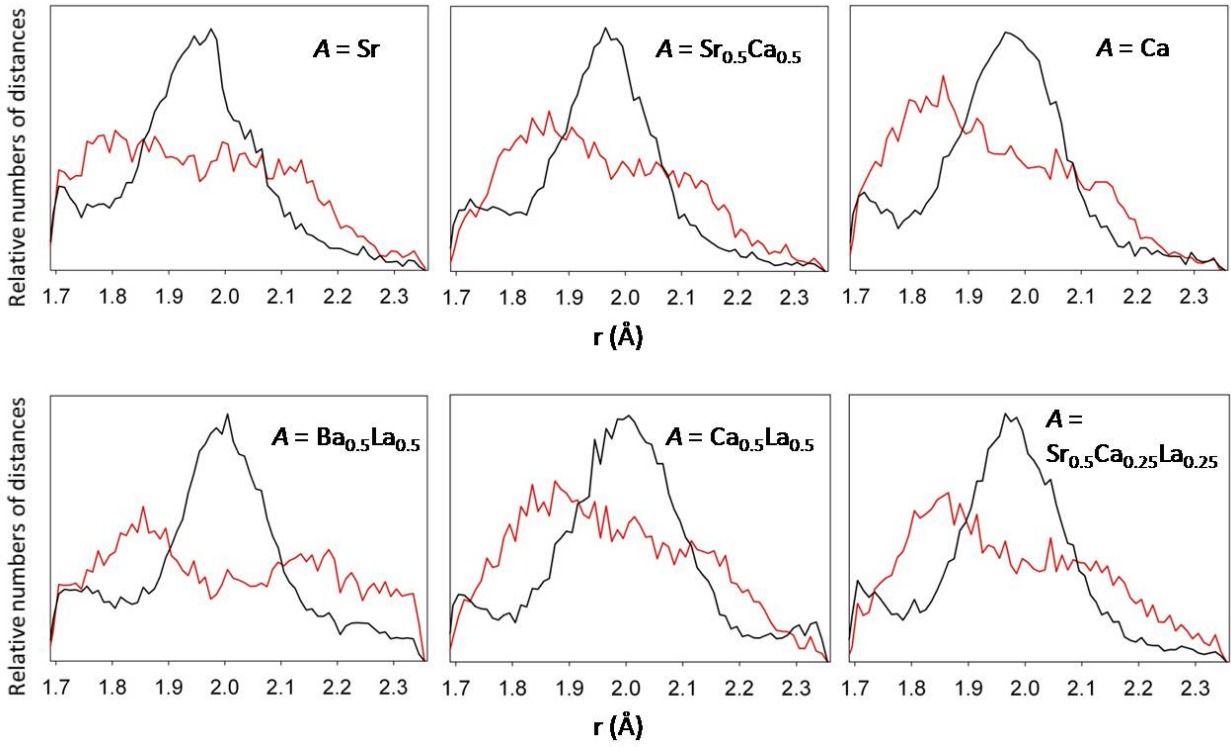


Figure 5. The distributions of Mn-O inter-atomic distances (red lines) and Ru-O inter-atomic distances (black lines) for all six compositions.

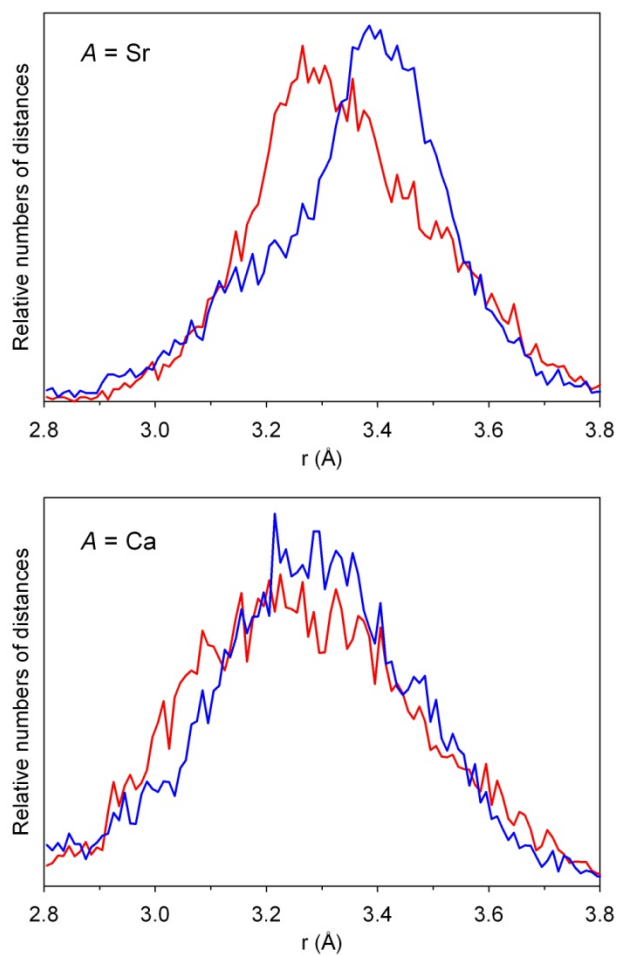


Figure 6. The Mn-Sr (red) and Ru-Sr (blue) PPDFs for $\text{SrMn}_{0.5}\text{Ru}_{0.5}\text{O}_3$ and $\text{CaMn}_{0.5}\text{Ru}_{0.5}\text{O}_3$.

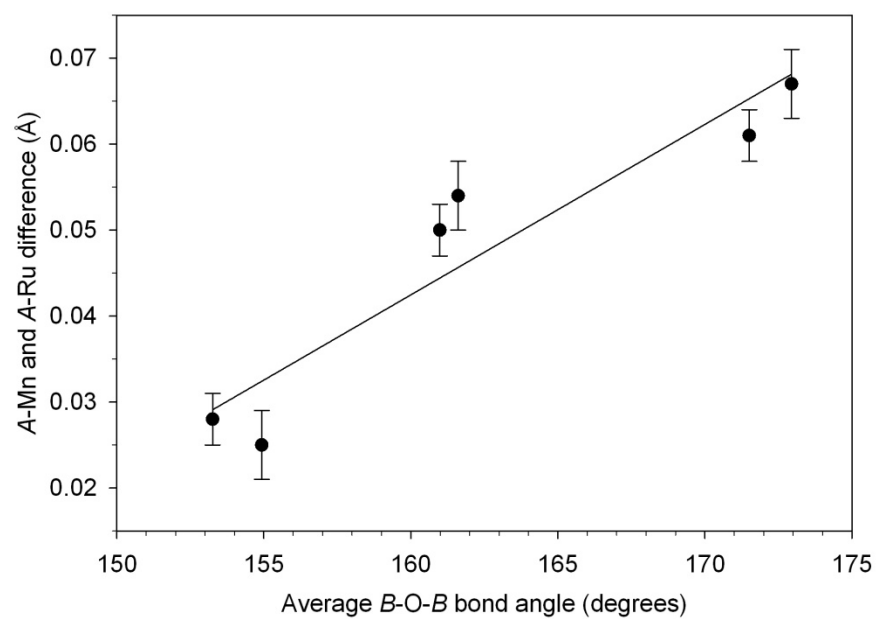


Figure 7. Correlation between the average $B-O-B$ bond angles of the average structures and the difference in the $A-Mn$ and $A-Ru$ nearest neighbor distances. The R^2 for the linear fit is 0.882.

References:

- 1) B. Raveau, A. Maignan, C. Martin, M. Hervieu, Chem. Mater, **10**, 2641 (1998).
- 2) T. Kimura, S. Kawamoto, I. Yamada, M. Azuma, M. Takano, Y. Tokura, Phys. Rev. B **67**, 180401 (2003).
- 3) T. Kimura, T. Goto, H. Shintani, K. Ishizaka, T. Arima, and Y. Tokura, Nature **426**, 55 (2003).
- 4) R. S. Singh, V. R. R. Medicherla, K. Maiti, Appl Phys. Lett. **91**, 132503 (2007).
- 5) I. I. Mazin, D. J. Singh, Phys. Rev. B **56**, 2556 (1997).
- 6) Y. Maeno, H. Hashimoto, K. Yoshida, S. Nishizaki, T. Fujita, J. G. Bednorz, F. Lichtenberg, Nature **372**, 532 (1994).
- 7) M. Yokoyama, C. Satoh, A. Saitou, H. Kawanaka, H. Bando, K. Ohoyama, Y. Nishihara, J. Phys. Soc. Jpn. **74**, 1706 (2005).
- 8) G. Cao, S. Chikara, X. N. Lin, E. Elhami, V. Durairaj, P. Schlottmann, Phys. Rev. B **71**, 035104 (2005).
- 9) T. Taniguchi, S. Mizusaki, N. Fukuoka, Y. Nagata, Y. Noro, H. Samata, J. Magn. Magn. Mater. **310**, 1067 (2007).
- 10) T. Taniguchi, S. Mizusaki, N. Okada, Y. Nagata, S. H. Lai, M. D. Lan, N. Hiraoka, M. Itou, Y. Sakurai, T. C. Ozawa, Y. Noro, H. Samata, Phys. Rev. B **77**, 014406 (2008).
- 11) S. Kolesnik, B. Dabrowski, O. Chmaissem, Phys. Rev. B **78**, 214425 (2008).
- 12) H. Kawanaka, M. Yokoyama, A. Noguchi, H. Bando, Y. Nishihara, J. Phys.: Condens. Matter **21**, 296002 (2009).
- 13) L. Wang, L. Hua, L. F. Chen, J. Phys.: Condens. Matter **21**, 495501 (2009).
- 14) D. H. Kim, S. M. Lee, S. Kolesnik, B. Dabrowski, B.-G. Park, J.-Y. Kim, J. Lee, B. I. Min, J.-S. Kang, J. Appl. Phys. **107**, 09E137 (2010).
- 15) K. Horiba, H. Kawanaka, Y. Aiura, T. Saitoh, C. Satoh, Y. Kikuchi, M. Yokoyama, Y. Nishihara, R. Eguchi, Y. Senba, H. Ohashi, Y. Kitajima, S. Shin, Phys. Rev. B **81**, 245127 (2010).
- 16) P. M. Woodward, J. Goldberger, M. W. Stoltzfus, H. W. Eng, R. A. Ricciardo, P. N. Santhosh, P. Karen, A. R. Moodenbaugh, J. Am. Ceram. Soc. **91**, 1796 (2008).

- 17) R. A. Ricciardo, H. L. Cuthbert, P. M. Woodward, Q. Zhou, B. J. Kennedy, Z. Zhang, M. Avdeev, L.-Y. Jang, Chem. Mater. **22**, 3369 (2010).
- 18) E. Granado, Q. Huang, J. W. Lynn, J. Gopalakrishnan, K. Ramesha, Phys. Rev. B **70**, 214416 (2004).
- 19) R. O. Bune, M. V. Lobanov, G. Popov, M. Greenblatt, C. E. Botez, P. W. Stephens, M. Croft, J. Halderman, G. Van Tendeloo, Chem. Mater. **18**, 2611 (2006).
- 20) B. H. Toby, EXPGUI, a graphical user interface for GSAS. J Appl. Crystallogr. **34**, 210 (2001).
- 21) A. C. Larson, R. B. Von Dreele, General Structure Analysis System (GSAS), Los Alamos National Laboratory Report LAUR 86-748 (2004).
- 22) P. F. Peterson, M. Gutmann, Th. Proffen, S. J. L. Billinge, J. Appl. Cryst. **33**, 1192 (2000).
- 23) A. P. Hammersley, ESRF Internal Report, ESRF98HA01T, FIT2D V9.129 Reference Manual V3.1 (1998).
- 24) A. P. Hammersley, S. O. Svensson, M. Hanfland, A. N. Fitch, D Hausermann, High Pressure Research, **14**, 235-248 (1996).
- 25) X. Qiu, J. W. Thompson, S. J. L. Billinge, J. Appl. Cryst. **37**, 678 (2004).
- 26) C. L. Farrow, P. Juhas, J. W. Liu, D. Bryndin, E. S. Bozin, J. Bloch, Th. Proffen, S. J. L. Billinge, J. Phys.: Condens. Matter **19**, 335219 (2007).
- 27) M. G. Tucker, D. A. Keen, M. T. Dove, A. L. Goodwin, Q. Hui, J. Phys.: Condens. Matter **19**, 335218 (2007).
- 28) B. J. Kennedy, Q. Zhou, Solid State Comm. **147**, 208 (2008).
- 29) M. W. Lufaso, P. M. Woodward, J. Goldberger, J. Solid State Chem. **177**, 1651 (2004).
- 30) T. Horikubi, N. Kamegashira, Mater. Chem. Phys. **65**, 316 (2000).
- 31) K. Shahzad, R. Shaheen, M. Nasir Khan, J. Bashir, J. Phys. D: Appl Phys. **41**, 175413 (2008).
- 32) See EPAPS Document No. [*number to be inserted by publisher*] for CIF files of the six compounds. For more information on EPAPS, see <http://www.aip.org/pubservs/epaps.html>.
- 33) N. E. Brese, M. O'Keeffe. Acta Cryst. **B 47**, 192-197 (1991).